

LDTrack: Dynamic People Tracking by Service Robots using Diffusion Models

Angus Fung · Beno Benhabib · Goldie Nejat

Abstract

Tracking of dynamic people in cluttered and crowded human-centered environments is a challenging robotics problem due to the presence of intraclass variations including occlusions, pose deformations, and lighting variations. This paper introduces a novel deep learning architecture, using conditional latent diffusion models, the Latent Diffusion Track (*LDTrack*), for tracking multiple dynamic people under intraclass variations. By uniquely utilizing conditional latent diffusion models to capture temporal person embeddings, our architecture can adapt to appearance changes of people over time. We incorporated a latent feature encoder network which enables the diffusion process to operate within a high-dimensional latent space to allow for the extraction and spatial-temporal refinement of such rich features as person appearance, motion, location, identity, and contextual information. Extensive experiments demonstrate the effectiveness of *LDTrack* over other state-of-the-art tracking methods in cluttered and crowded human-centered environments under intraclass variations. Namely, the results show our method outperforms existing deep learning robotic people tracking methods in both tracking accuracy and tracking precision with statistical significance.

Keywords Robotic Person Tracking · Service Robots · Diffusion Models · Intraclass Variations · Cluttered and Crowded Environments

1 Introduction

Service robots need to be able to autonomously track multiple dynamic people in diverse cluttered and crowded human-centered environments to initiate social or physical human-robot interactions (HRI). Such applications range from product searches in retail stores (Dworakowski et al. 2023); directional guidance in airports (Agrawal and Lal 2021) and hospitals (Kollmitz et al. 2019; Vasquez et al. 2017); domestic assistance for elderly and impaired individuals (Sanz et al. 2015); activity/task recognition (T. Liu et al. 2022); robot exploration (Tan et al. 2023) and navigation (Gupta et al. 2020; Royer et al. 2007; Haitong Wang et al. 2024; Xue et al. 2024); to person following (Pang et al. 2020; Vo et al. 2014; Weber et al. 2018). These environments present the challenge of intraclass variations, which encompass differences in observations of the same people. In particular, in tracking of people, intraclass variations are a result of occlusions, clothing deformations, body articulation, or changes in lighting conditions, which may result in varying appearances for the same individual across different RGB image frames (Fung et al. 2023; Hanxiao Wang et al. 2018; Yan et al. 2023).

The majority of existing people tracking methods used by robots in human-centered environments require a separate detection system for identification and localization of people and a separate tracking system to track the detected movements of these people over time, while maintaining their identity across different observations (Agrawal and Lal 2021; Kollmitz et al. 2019; Pang et al. 2020; Sanz et al. 2015; Vasquez et al. 2017; Vo et al. 2014; Weber et al. 2018). However, as detection is performed independently on each image frame, these detectors do

not have the temporal coherence that is essential for tracking under intraclass variations (Lu et al. 2020). The reliance of these tracking techniques on this isolated frame-by-frame detection can become a bottleneck if the detector fails to identify a person in a subset of the consecutive frames.

A handful of multi-object tracking (MOT) approaches have been developed (Lu et al. 2020; Voigtlaender et al. 2019; Meinhardt et al. 2022; Peize Sun et al. 2021; Zeng et al. 2022; Chuang et al. 2024; Zhou et al. 2020; Chaabane et al. 2021) which incorporate joint detection and tracking (JDT) models to unify these two stages within a single deep learning (DL) network to solve the general object tracking problem. These models utilize proposal boxes that are learned during training to predict the locations of people. However, large datasets are needed to learn these boxes effectively (Dai et al. 2022). For robotics applications with sparse data, this may result in model overfitting, thereby reducing adaptability to diverse and dynamic human-centered settings. Moreover, these JDT methods rely on a fixed number of proposal boxes (Carion et al. 2020) which are for specific sizes and locations of objects including people, this can be challenging to use in crowded environments where people overlap each other significantly. Thus, JDT models cannot adapt to variations in crowd density, especially when they significantly differ from the training datasets used.

Recently, diffusion models have been proposed for a number of vision-based tasks, including image synthesis (Rombach et al. 2022), inpainting (Lugmayr et al. 2022), object detection (Chen et al. 2023), and object tracking (Luo et al. 2023). Diffusion models are deep generative models which generate data by perturbing an initial input through a forward diffusion process involving Gaussian noise, and a reverse diffusion process using a

Markov chain to iteratively recover the original data (Sohl-Dickstein et al. 2015). Diffusion models can be used to generalize tracking across scenes with varying levels of crowd density by iteratively refining proposal boxes generated from noise which do not need to be trained. This is advantageous over the aforementioned learned proposal boxes.

While both (Chen et al. 2023) and (Luo et al. 2023) proposed the use of diffusion models for object detection and tracking, these methods use static embeddings that cannot be updated based on information from previous RGB frames. In contrast, temporal person embeddings, which accumulate information over time, are important for robust person representations in order to adapt to intraclass variations. Diffusion models have the potential to capture temporal embeddings that are person specific by conditioning on past embeddings from each person’s respective tracks, *i.e.* track-conditioned. To effectively capture appearance and contextual features over time, the diffusion process needs to use a latent embedding space rather than directly applying the diffusion process over the person bounding box pixel space. To-date, diffusion methods have not yet been explored for the robotic problem of dynamic people tracking.

In this paper, we present a novel people tracking architecture for mobile service robots using conditional latent diffusion models, which we name Latent Diffusion Track (*LDTrack*), to solve the robotic problem of tracking multiple dynamic people under intraclass variations. The main contributions of this paper are: 1) the development of a new people tracking architecture utilizing a joint detection and tracking framework for people tracking by robots in crowded and cluttered environments; 2) the first use of track-conditioned latent diffusion models to capture temporal person embeddings defined as *person track embeddings* – these embeddings are specific to each person and accumulate temporal information of people appearance changes over time; and, 3) the inclusion of a latent feature encoder network to allow for the extraction and spatial-temporal refinement of rich person features including person appearance, motion, location, identity, and contextual information in a high-dimensional latent space.

2 Related Work

In this section, we discuss the existing literature on: 1) joint multi-object detection and tracking methods, 2) robotic detection and tracking of people in human-centered environments, and 3) diffusion model methods.

2.1 Joint Multi-Object Detection and Tracking Methods

Recent research in multi-object tracking (MOT) utilizes joint detection and tracking (JDT) methods which integrate detection and tracking within a single network (Lu et al. 2020; Voigtlaender et al. 2019; Meinhardt et al. 2022; Peize Sun et al.

2021; Zeng et al. 2022; Chuang et al. 2024; Zhou et al. 2020; Chaabane et al. 2021). While these methods have been designed for tracking general objects, they have mainly been evaluated on urban outdoor datasets with pedestrians and vehicles (Voigtlaender et al. 2019). JDT methods are promising for our robotics problem as a unified network improves temporal coherence as well as computational efficiency (Lu et al. 2020). Both (Lu et al. 2020) and (Voigtlaender et al. 2019) extended off-the-shelf object detectors to perform object tracking. For example, in (Lu et al. 2020), RetinaTrack was developed to improve object tracking efficiency in mission critical tasks such as autonomous driving. RetinaTrack extended the RetinaNet detector (Lin et al. 2020), allowing the detector to extract instance-level object features for data association. RetinaTrack was evaluated on the Waymo Open dataset (Pei Sun et al. 2020), specifically the vehicle class, taken from urban outdoor environments. Similarly, in (Voigtlaender et al. 2019), Track R-CNN (Track Region-based CNN) was developed to jointly perform detection, tracking and segmentation of general objects such as vehicles, with the objective of improving object tracking by considering pixel-level information. Namely, Track R-CNN extended the Mask R-CNN detector (He et al. 2017) by incorporating an associating head for data association and 3D convolution layers for capturing temporal information across frames. Track R-CNN was evaluated on the KITTI MOTs dataset (Voigtlaender et al. 2019) consisting of both vehicles and pedestrians taken from urban outdoor environments.

In (Meinhardt et al. 2022; Peize Sun et al. 2021; Zeng et al. 2022), TrackFormer, TransTrack, and MOTR were introduced as methods using DETection TRANSformers (DETR) (Carion et al. 2020). Their objective was to improve object tracking efficiency. Both TrackFormer (Meinhardt et al. 2022) and MOTR (Zeng et al. 2022) used track queries, which are representations that track objects and maintain their identities across frames. TransTrack (Peize Sun et al. 2021) used object features from previous RGB frames as track queries, and generated parallel sets of detection and tracking boxes which were then combined using the Hungarian algorithm for data association. All three methods were evaluated on the MOT17 (Dendorfer et al. 2021) and MOT20 (Voigtlaender et al. 2019) datasets, consisting of pedestrians in outdoor urban environments.

2.2 Robotic Tracking of People

Existing people tracking methods for robotic applications in indoor environments have primarily used tracking-by-detection (TBD) methods to track multiple people (Kollmitz et al. 2019; Munaro and Menegatti 2014; Pang et al. 2020; Pereira et al. 2022; Sanz et al. 2015; S. Sun et al. 2019; Taylor and Riek 2022; Vasquez et al. 2017; Vo et al. 2014; Weber et al. 2018). TBD consist of three main stages (Murray 2017): 1) a static frame-to-

frame person detector, 2) prediction of a new person location from previous frames, and 3) data association between frames of predicted and detected person locations. The static frame-to-frame detectors can broadly be divided into: 1) classical methods such as Support Vector Machines (SVMs) with Histogram of Oriented Gradients (HOG) features (Munaro and Menegatti 2014; Sanz et al. 2015; Vo et al. 2014); or 2) deep learning methods such as a) Faster R-CNN (FRCNN) (Kollmitz et al. 2019; Vasquez et al. 2017), b) You Only Look Once (YOLO) (Pang et al. 2020; Pereira et al. 2022; Pinto et al. 2023; Taylor and Riek 2022), and c) Single Shot MultiBox Detector (SSD) (Weber et al. 2018). The prediction stage is used to predict locations of people in future frames using Kalman filters (KF) (Kollmitz et al. 2019; Munaro and Menegatti 2014; Pang et al. 2020; Pereira et al. 2022; Pinto et al. 2023; Sanz et al. 2015; S. Sun et al. 2019; Taylor and Riek 2022; Vo et al. 2014; Weber et al. 2018). The data association stage then matches predictions with new detections using the Hungarian algorithm (Pereira et al. 2022; Vo et al. 2014), the Mahalanobis distance (Kollmitz et al. 2019; Munaro and Menegatti 2014; Pinto et al. 2023; S. Sun et al. 2019), the Euclidean distance (Pereira et al. 2022; Sanz et al. 2015), the Intersection over Union (IoU) distance (Pang et al. 2020; Pereira et al. 2022), or by probability gating (Weber et al. 2018). These methods considered various types of intraclass variations including: partial and/or full occlusions (Kollmitz et al. 2019; Munaro and Menegatti 2014; Pang et al. 2020; Pereira et al. 2022; Pinto et al. 2023; Sanz et al. 2015; S. Sun et al. 2019; Taylor and Riek 2022; Vasquez et al. 2017; Vo et al. 2014; Weber et al. 2018), varying lighting (Vo et al. 2014), and varying poses (Pereira et al. 2022; Vo et al. 2014).

Service robots have used people tracking methods for assistance such as in hospitals and airports (Kollmitz et al. 2019; Taylor and Riek 2022; Vasquez et al. 2017) and in the homes of older adults (Sanz et al. 2015). For example, in both (Kollmitz et al. 2019; Vasquez et al. 2017), a people tracking approach was proposed for robots to find people using mobility aids in populated environments. A FRCNN detector was trained on the Mobility Aids dataset (Vasquez et al. 2017) consisting of RGB-D images of people with different aids in a hospital obtained from a mobile robot. The detector was pretrained on ImageNet (Russakovsky et al. 2015). The position and velocity of a person were then tracked using an extended KF (EKF). For data association between tracks and observations, the pairwise Mahalanobis distances from the EKF were used. Experiments were conducted in an indoor hospital environment and included scenarios with partial person occlusions due to others. In (Taylor and Riek 2022), REGROUP was proposed for assistive robots to guide people in crowded airports. REGROUP detected people using YOLOv3 (Redmon and Farhadi 2018), and performed group data association utilizing KF. Crowd Indication Feature (CIF) was used to determine ego-centric distance metrics to detect

crowds. Individual people tracking within crowds was performed by utilizing spatial matrices for precise individual person localizations.

In (Sanz et al. 2015), a people tracking approach was proposed for service robots assisting the elderly and impaired in indoor cluttered environments. A robot used a Kinect RGB-D sensor for depth-based segmentation using Otsu's method to identify potential people and a SVM with HOG features for person detection. For tracking, a KF was used to predict position and velocity of people while a blob matching method based on Euclidean distance was used for data association. Experiments were conducted in an indoor home-like environment and included scenarios with partial person occlusion.

Service robots have also used people tracking methods for person following (Munaro and Menegatti 2014; Pang et al. 2020; Pinto et al. 2023; Weber et al. 2018). For example, in (Pang et al. 2020), a people tracking approach was proposed for a robot following a person in open outdoor environments with a stereo camera. The approach used a YOLO detector for people detection and a KF to predict future locations of people. Data association was performed by matching the detection with the highest IoU score to the predicted boxes from the KF. Experiments were conducted in an outdoor environment with scenarios of partial and full person occlusions.

In (Weber et al. 2018), a people tracking approach was proposed for a robot following a person in unknown crowded environments with an RGB camera. The approach used the SSD (W. Liu et al. 2016) detector for head detection, followed by a KF to predict future people locations. Data association was performed by matching the nearest detection to these predictions based on probability within a specified range. Experiments were conducted in an indoor environment with a robot following a target person who was occluded by others.

In (Munaro and Menegatti 2014), a people tracking approach for a mobile robot used RGB-D data and depth-based sub-clustering to identify and follow individuals. HOG detection was used to detect people's heads within clusters. The method combined multiple clusters together, which could be subdivided due to occlusions, for effective tracking in crowded and occluded environments. An Unscented KF was integrated for estimating the positions and velocities of people. The Mahalanobis distance was used for robust data association. Experiments were conducted in crowded indoor environments under varying lighting conditions.

In (Pinto et al. 2023), a people tracking approach was presented for a companion robot to track, follow and re-identify multiple people. The method detected people in RGB images using YOLOv3 (Redmon and Farhadi 2018), and used TriNet (Yuan et al. 2020) for re-identification and KF for predicting the positions of tracked people. Experiments were conducted in an indoor home environment with occlusions and appearance

changes.

Several people tracking methods have also been utilized in general indoor environments (Pereira et al. 2022; S. Sun et al. 2019; Vo et al. 2014). For example, in (Vo et al. 2014), a people tracking approach for a mobile robot was proposed for tracking people under varying poses and appearances. The robot used a Kinect RGB-D sensor for depth-based skin color segmentation which was combined with the Viola-Jones algorithm (Viola and Jones 2001) for face detection, while the upper body detection used an SVM classifier with HOG features extracted from RGB images. The system primarily relied on a fast-compressive tracker, switching to a KF in cases of significant occlusions. For data association, the Hungarian algorithm was used to match detections to existing tracks based on an overlap ratio. Experiments were conducted in an indoor environment under varying lighting conditions with person occlusion.

In (Pereira et al. 2022), two people tracking approaches for mobile robots were compared: 1) SORT (Simple Online and Real-Time Tracking) (Bewley et al. 2016), and 2) Deep-SORT (Wojke et al. 2017). SORT uses a KF for motion prediction, and the Hungarian algorithm for data association, while Deep-SORT extends SORT by integrating a CNN to extract person features. Both methods used the YOLOv3 detector (Redmon and Farhadi 2018) to identify bounding boxes for detected people in RGB images. A new set of data association cost matrices were proposed such as IoU, and Euclidean distances. Experiments were conducted in an indoor campus environments with scenarios consisting of people in sitting and leaning over poses as well as occluding each other.

Lastly, in (S. Sun et al. 2019), an RGB-D multi-person tracking approach was developed for mobile robots in crowded environments. The approach used a deformable part model for person detection and a Gaussian model based on depth values to identify partially occluded people. Data association was performed by matching detections with KF predictions based on Mahalanobis distance. Experiments were conducted on the KTP dataset (Munaro and Menegatti 2014) containing crowds in an indoor office.

2.3 Diffusion Models

Diffusion models are deep generative models which operate by gradually transforming a distribution of random noise into a distribution of data (i.e., images or features) through a Markov chain process (Sohl-Dickstein et al. 2015). This process involves a forward diffusion phase, which adds noise to the data, and a reverse diffusion phase, which learns to reverse this process to generate or reconstruct data (Rombach et al. 2022). Diffusion models have been applied to a number of vision tasks, including image synthesis, *e.g.*, (Rombach et al. 2022), inpainting *e.g.*, (Lugmayr et al. 2022), and more recently in object detection

(Chen et al. 2023) and object tracking (Luo et al. 2023). Diffusion methods can be conditional and therefore depend on specific conditions to consider more information. For example, conditioning on text descriptions for image generation (Rombach et al. 2022), or conditioning on the visible portion of the image for image inpainting (Lugmayr et al. 2022; Rombach et al. 2022). Diffusion models can also be latent, where the diffusion process occurs in a transformed feature space rather than directly in the pixel space (Rombach et al. 2022).

A conditional latent diffusion model was used in (Rombach et al. 2022) for high-resolution image synthesis by using a sequence of denoising autoencoders. The integration of cross-attention layers enabled the model to handle conditioning inputs such as text descriptions and visible portions of an image. In (Lugmayr et al. 2022), a conditional diffusion model was used for free-form inpainting of images to add missing content to images within regions defined by arbitrary binary masks. The model used a pretrained unconditional diffusion model, conditioning the generation process by sampling unmasked regions, thereby using the visible parts of the image as the condition.

In (Chen et al. 2023), an image-conditioned diffusion model was used for object detection by evolving random boxes from a random distribution to precise detections. During training, the model learned to reverse the diffusion of object boxes from ground truth to randomness. In the inference stage, the model progressively refined randomly generated boxes into predicted bounding boxes, conditioned on the input image. In (Luo et al. 2023), an image-conditioned diffusion model was also used for object tracking by transforming bounding box pairs generated from noise into accurate ground-truth boxes across adjacent video frames. The architecture integrated a YOLOX feature backbone and a data association denoising head. The backbone extracted object features from adjacent frames, which were then refined by the diffusion head through a spatial-temporal fusion module. During training, the model learned to reverse the diffusion of paired object boxes from a random distribution to their ground truth state in pixel space. During inference, the model refined a set of paired randomly generated boxes to object tracks, conditioned on both the current and previous frames.

2.4 Summary of Limitations

As existing robotic people tracking methods are tracking-by-detection methods, they do not consider temporal coherence, as the detector and tracker function independently. The detector processes each frame in isolation, which can lead to inaccuracies in consistently identifying individuals across time, particularly in scenarios with occlusions, lighting changes, and with individuals that have similar appearances. These inaccuracies can result in tracking errors such as identity switches or loss of tracking continuity (Lu et al. 2020). Alternatively, MOT methods (Lu et

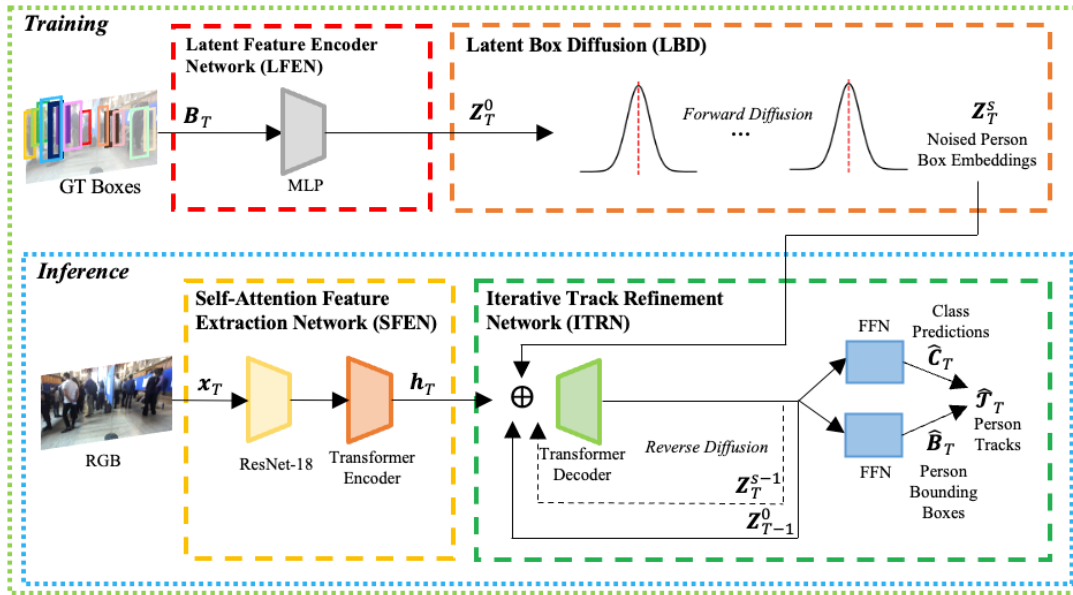


Fig. 1 Proposed *LDTrack* architecture

al. 2020; Voigtlaender et al. 2019; Meinhardt et al. 2022; Peize Sun et al. 2021; Zeng et al. 2022; Chuang et al. 2024; Zhou et al. 2020; Chaabane et al. 2021) have incorporated JD_T within a single network architecture. These methods utilize transformer models which use learned proposal boxes for tracking. However, they require large datasets to learn effectively (Dai et al. 2022). Robotic datasets are typically small, leading to potential overfitting. Furthermore, MOT methods are constrained to track from a fixed number of learnable proposal boxes, restricting their ability to adapt to scenes with varying person densities (Chen et al. 2023).

On the other hand, diffusion models have the potential to track people from parameter-free proposal boxes by initializing these boxes from Gaussian noise. Thus, not requiring large datasets for the training of learned proposal boxes as is needed for JD_T methods. These boxes can be used to track individuals in environments of any density or complexity, as they can be iteratively refined to track people at any location or of any configuration within the image. However, diffusion models have only been applied to multi-object tracking (Luo et al. 2023) and have not yet considered people tracking or intraclass variations. Thus, existing methods cannot be directly applied to address the robotic problem of tracking people in cluttered and crowded environments under intraclass variations.

3 People Tracking Methodology

We propose a novel joint people detection and tracking architecture for tracking multiple dynamic people in cluttered and crowded human-centered environments. The proposed architecture, *LDTrack*, represents the tracking problem as a generative

task using conditional latent diffusion models, Fig. 1. Namely, *LDTrack* consists of training and inference sub-systems. The *Inference Subsystem* uses RGB images to determine person feature embeddings which represent person appearance and contextual information via the *Self-Attention Feature Extraction Network (SFEN)* module. We use RGB images as they provide the necessary visual features to distinguish between different individuals, for example doctors, nurses, and patients in a hospital. The person feature embeddings are utilized by the *Iterative Track Refinement Network (ITRN)* module to determine person track embeddings. These track embeddings, specific to each individual being tracked, accumulate temporal information by updating over time, capturing person appearance, contextual, motion, location, and identity information. The person track embeddings are used by the two feed-forward neural networks (FFN) for the identification of both individual person bounding boxes and class predictions (person or background). The final output of *LDTrack* is the person tracks, defined as ordered sequences of bounding boxes that represent individual person trajectories within the environment. These tracks are updated based on the identified bounding boxes and class predictions.

The *Training Subsystem* uses the *Latent Feature Encoder Network (LFEN)* module to transform ground truth (GT) person bounding boxes into a latent space representation of higher dimension. This enables the diffusion model to regress richer features such as person appearance, motion, and contextual features in order to maintain accurate identification and tracking of individuals due to changes in their appearances from variations in occlusion, lighting, and poses. The *Latent Box Diffusion (LBD)* module introduces Gaussian noise to the latent representations to generate noised person box embeddings, which executes the forward diffusion step of the diffusion model framework, Fig. 1.

The noised person box embeddings are then used by the *ITRN* module, which reverses the diffusion process, to update and maintain person tracks. The following subsections discuss the main modules of the inference and training subsystems of *LDTrack* in detail.

3.1 Inference Subsystem

The *Inference Subsystem* of the *LDTrack* architecture is used for real-time people tracking in cluttered and crowded human-centered environments. It contains the *SFEN* and *ITRN* modules. The output of the *ITRN* consists of person tracks, representing individual person trajectories within the environment.

3.1.1 Self-Attention Feature Extraction Network (SFEN)

The *SFEN* module extracts person feature (appearance and contextual information) embeddings, \mathbf{h}_T , from multiple individuals in an RGB image, \mathbf{x}_T , at discrete time T . *SFEN* consists of a ResNet network (He et al. 2016), defined as \mathbf{f}_{CNN} , and a transformer encoder (Zhu et al. 2021), defined as \mathbf{f}_{ENC} . We use a ResNet-18 network to extract initial person features as it is computationally efficient to meet the inference requirements of robotic applications (Fung et al. 2023). Our ResNet-18 network consists of 5 convolution blocks, a fully connected (FC) and a SoftMax layer. The skip connections between the convolutional layers create shortcuts to bypass one or more layers (He et al. 2016). They are used herein to ensure that the network retains low-level details such as color and texture which are crucial for distinguishing between different individuals.

The transformer encoder receives the feature map from the last convolution block of ResNet-18 to extract \mathbf{h}_T . We adapted the transformer architecture from (Zhu et al. 2021), as it utilizes deformable attention modules which allow the encoder to efficiently sample a sparse set of discriminative person features that are most relevant to people tracking under varying environment conditions. The output of the encoder is the person feature embeddings at time T :

$$\mathbf{h}_T = \mathbf{f}_{SFEN}(\mathbf{x}_T) = (\mathbf{f}_{ENC} \circ \mathbf{f}_{CNN})(\mathbf{x}_T). \quad (1)$$

3.1.2 Iterative Track Refinement Network (ITRN)

The *ITRN* module consists of a transformer decoder, followed by two FFNs to generate person track embeddings, $\mathbf{Z}_T^{s_0}$, and corresponding person tracks, $\hat{\mathcal{T}}_T = \{\hat{\mathcal{T}}_{k_i, T}\}$, where $k_i \in \mathcal{K}_T$ is the subset of people visible in the RGB frame at time T . s_0 denotes the final step of the reverse diffusion process, where the model has iteratively reconstructed the person track embeddings from its noised state. $\hat{\mathcal{T}}_{k_i, T} = (\hat{\mathbf{b}}_{k_i, T_1}, \hat{\mathbf{b}}_{k_i, T_2}, \dots, \hat{\mathbf{b}}_{k_i, T})$ represents the trajectory of a person with identity k_i over timesteps up to the current time T . The transformer decoder takes as inputs: 1) the

noised person box embeddings of size N_{ns} , $\mathbf{Z}_T^s \sim \mathcal{N}(\mathbf{0}, \mathbf{I})$, initialized from a multivariate normal distribution, 2) person track embeddings $\mathbf{Z}_{T-1}^{s_0}$ from the previous timestep of size N_{tk} , and 3) person feature embeddings \mathbf{h}_T from the *SFEN* module. The decoder produces a set of output person track embeddings $\mathbf{Z}_T^{s_0}$ of size $N_{ns} + N_{tk}$. The noised person box embeddings \mathbf{Z}_T^s are the starting point for the reverse diffusion process, which systematically denoises and refines these embeddings into the final set of output person box embeddings $\mathbf{Z}_T^{s_0}$. Person box embeddings represent probabilistic proposals for potential person locations (position and scale) within a frame.

The structure of the transformer decoder is an extension of the decoder in (Zhu et al. 2021). It incorporates six decoder layers with each layer containing a combination of multi-head attention mechanisms and FFNs. Unique to our approach, we utilize noised box embeddings \mathbf{Z}_T^s and track embeddings from the previous timestep $\mathbf{Z}_{T-1}^{s_0}$ as the inputs instead of learned position embeddings which were used in (Zhu et al. 2021). The transformer decoder performs the reverse diffusion process, with \mathbf{Z}_T^s and $\mathbf{Z}_{T-1}^{s_0}$ concatenated at the input. The inputs then undergo cross-attention with the person feature embeddings \mathbf{h}_T from *SFEN* to produce person track embeddings \mathbf{Z}_T^0 , allowing the decoder to focus on specific regions of an RGB image. These embeddings can be refined iteratively by reversing the diffusion steps in a sequential manner, starting from $s = S$ until reaching the step $s = s_0 = 0$ through the \mathbf{f}_{ITRN} network:

$$\mathbf{Z}_T^{s-1} = \mathbf{f}_{ITRN}(\mathbf{Z}_T^s, \mathbf{Z}_{T-1}^{s_0}; \mathbf{h}_T), \quad (2)$$

where the person track embeddings \mathbf{Z}_T^{s-1} at diffusion step $S - 1$ are obtained from step S . The iterative refinement process allows for incremental improvements of tracking in latent space, enabling *LDTrack* to adapt to changes in individual appearances as well as accommodate diverse spatial configurations of varying crowd densities. Thus, these track embeddings are refined both spatially and temporally to learn and accumulate temporal person features that are robust under intraclass variations. Spatial refinement is achieved through the aforementioned iterative process of reversing the diffusion steps, and temporal refinement is achieved by conditioning on the person track embeddings from previous timesteps.

After iterative person track refinement, the final set of output person track embeddings \mathbf{Z}_T^0 , are then passed into two separate FFNs. One FFN is used for person class prediction $\hat{\mathbf{c}}_{k_i, T}$ (person or background), and the other for person bounding box prediction $\hat{\mathbf{b}}_{k_i, T}$. The final output $\hat{\mathcal{Y}}_T$ of the FFN consists of the predicted person bounding box and class pairs:

$$\hat{\mathcal{Y}}_T = \{\hat{\mathbf{y}}_{k_i, T}\}_{i=1}^{N_{ns}+N_{tk}}, \mathbf{y}_{k_i, T} = (\hat{\mathbf{c}}_{k_i, T}, \hat{\mathbf{b}}_{k_i, T}). \quad (3)$$

Person tracks, which are ordered sequences of bounding boxes representing a person’s trajectory and their respective person track embeddings, can become inactive by no longer being

updated or tracked. Namely, they become inactive when the individual is no longer visible in an RGB image, for example, due to full occlusion. A track becomes inactive: if $p(\hat{\mathbf{c}}_{k,T}) < \sigma_{\text{cls}} = 0.4$ or if $\text{IoU} < \sigma_{\text{IoU}} = 0.9$ with other bounding boxes (Meinhardt et al. 2022). New person tracks $\hat{\mathbf{T}}_{k_i,T}$, $k_i \in \mathcal{K}_{\text{new}}$ are obtained from \mathbf{Z}_T^S for new detections, while existing person tracks $\hat{\mathbf{T}}_{k_i,T}$, $k_i \in \mathcal{K}_{T-1}$ are updated from $\mathbf{Z}_{T-1}^{S_0}$. A person track $\hat{\mathbf{T}}_{k_i,T}$ can be obtained using the predicted person bounding boxes $\hat{\mathbf{b}}_{k_i,T}$ from Eq. (3) as follows:

$$\hat{\mathbf{T}}_{k_i,T} = \begin{cases} \hat{\mathbf{T}}_{k_i,T-1} \cup \{\hat{\mathbf{b}}_{k_i,T}\}, & k_i \in \mathcal{K}_{T-1} \\ \{\hat{\mathbf{b}}_{k_i,T}\}, & k_i \in \mathcal{K}_{\text{new}} \end{cases}. \quad (4)$$

To handle temporary occlusions, where a person may be obscured from the view of the robot’s RGB camera for a short period of time, inactive person tracks are retained for an additional N_{reid} frames similar to (Meinhardt et al. 2022). Should the person reappear within this short time span, *LDTrack* can resume tracking without initializing a new person track for an existing person. These person tracks can be reactivated if their classification score $p(\hat{\mathbf{c}}_{k,T}) > \sigma_{\text{cls}}$, indicating a renewed confidence in the presence of a person (Meinhardt et al. 2022). Since person track embeddings from prior time steps undergo direct refinements, data association is implicitly achieved without any additional computational overhead. Thus, the final set of person tracks $\hat{\mathcal{T}}_T$ obtained from the inference subsystem is:

$$\hat{\mathcal{T}}_T = \{\hat{\mathbf{T}}_{k_i,T}\}, k_i \in \mathcal{K}_T = \mathcal{K}_{T-1} \cup \mathcal{K}_{\text{new}}. \quad (5)$$

3.2 Training Subsystem

The *Training Subsystem* uses both the *LFEN* and *LBD* modules to produce noised person box embeddings \mathbf{Z}_T^S . The *ITRN* then transforms these noised person box embeddings \mathbf{Z}_T^S into person bounding box predictions, $\hat{\mathbf{Y}}_T$, to optimize a set prediction loss.

3.2.1 Latent Feature Encoder Network (LFEN)

The *LFEN* module converts ground truth (GT) person bounding boxes into a higher dimensional latent space. $\mathbf{B}_T \in \mathcal{B}$ is the set of GT person bounding boxes at discrete time T , and $\mathbf{b}_{k,T} \in \mathcal{B}_T$ represent the person bounding box with identity $k \in \mathcal{K}$, where $\mathbf{b}_{k,T}$ represents the 2D location of the center (x, y) and the width w and height h of the bounding box, respectively. The latent representation of the GT person bounding boxes $\mathbf{z}_{k,T} \in \mathbb{R}^D$ are obtained by passing the set of GT bounding boxes $\{\mathbf{b}_{k,T}\}$ through the multi-layer perception (MLP), \mathbf{f}_{LFEN} :

$$\mathbf{z}_{k,T} = \mathbf{f}_{\text{LFEN}}(\mathbf{b}_{k,T}). \quad (6)$$

We designed the MLP to consist of three fully connected layers, each with a hidden layer dimension of size D . To account

for the varying number of ground truth boxes $\mathbf{b}_{k,T}$ across different RGB frames and also maintain consistent input dimensions for the *LBD* module, we pad \mathbf{B}_T to the fixed size N_{ns} , which is the same size as the noised person box embeddings (Chen et al. 2023). This is achieved by initializing these GT bounding boxes from a normal distribution:

$$\mathbf{b}_{\text{pad}} \sim \mathcal{N}(0.5, \sigma^2), \quad (7)$$

where $\sigma = 1/6$ was chosen such that 3σ represents a range between 0 and 1. The output set of latent representations of person box embeddings $\mathbf{Z}_T = \{\mathbf{z}_{k,T}\}_{i=1}^{N_{\text{ns}}}$ is then provided to the *LBD* module.

3.2.2 Latent Box Diffusion (LBD)

The objective of the *LBD* module is to initiate the forward diffusion process by converting the set of latent representations of person box embeddings \mathbf{Z}_T to noised person box embeddings \mathbf{Z}_T^S . This is achieved through a Markovian-chain driven diffusion forward process by systematically applying Gaussian noise to the data according to the noise variance schedule β_1, \dots, β_S (Ho et al. 2020):

$$q(\mathbf{Z}_T^s | \mathbf{Z}_T^0) = \mathcal{N}(\mathbf{Z}_T^s | \sqrt{\bar{\alpha}_s} \mathbf{Z}_T^0, (1 - \bar{\alpha}_s) \mathbf{I}), \quad (8)$$

where $q(\mathbf{Z}_T^s | \mathbf{Z}_T^0)$ is the forward diffusion noise distribution of the person box embeddings \mathbf{Z}_T^s at diffusion step s given the initial person box embeddings; $\mathbf{Z}_T = \mathbf{Z}_T^0 = \{\mathbf{z}_{k,T}^0\}$ at step $s = 0$; $\alpha_s = 1 - \beta_s$; $\bar{\alpha}_s = \prod_{j=1}^s \alpha_j$; and \mathbf{I} is the identity matrix. α_s represents the proportion of the original embedding that is retained after noise has been applied and β_s represents the amount of noise being added at each step s in the diffusion process. The output set of noised person box embeddings, at the final step $s = S$, is $\mathbf{Z}_T^S = \{\mathbf{z}_{k,T}^S\}$. This output set is provided to the *ITRN* module.

3.2.3 Self-Attention Feature Extraction Network (SFEN)

The *SFEN* module is trained on pairs of consecutive RGB frames $(\mathbf{x}_{T-1}, \mathbf{x}_T)$ in order to learn temporal features of people as their appearance changes across RGB frames. The pair of frames is used in Eq. (1) to extract the corresponding person feature embeddings \mathbf{h}_{T-1} and \mathbf{h}_T . The person feature embeddings are then also provided to the *ITRN* module.

3.2.4 Iterative Track Refinement Network (ITRN)

The *ITRN* uses \mathbf{h}_{T-1} and \mathbf{h}_T to predict person class and bounding boxes which are used to optimize a set prediction loss. For \mathbf{x}_{T-1} , we use \mathbf{f}_{ITRN} to directly predict the person box embeddings $\mathbf{Z}_{T-1}^{S_0}$ within a single step of reverse diffusion using Eq. (2):

$$\mathbf{Z}_{T-1}^{S_0} = \mathbf{f}_{\text{ITRN}}(\mathbf{Z}_{T-1}^S; \mathbf{h}_{T-1}). \quad (9)$$

Namely, time $T - 1$ serves as the starting point for each RGB pair. As discussed in Section 3.1.2, the person box embeddings $\mathbf{Z}_{T-1}^{s_0}$ are passed into two separate FFNs for person bounding boxes $\hat{\mathbf{b}}_{k_i,T}$ and class predictions $\hat{\mathbf{c}}_{k_i,T}$. $\mathbf{Z}_{T-1}^{s_0}$ which satisfy the IoU and classification thresholds σ_{IoU} and σ_{cls} are retained as person track embeddings for the subsequent timestep. At T , \mathbf{f}_{ITRN} is again used to directly predict person box embeddings $\mathbf{Z}_T^{s_0}$ within a single step from $\mathbf{Z}_{T-1}^{s_0}$ using Eq. (2):

$$\mathbf{Z}_T^{s_0} = \mathbf{f}_{ITRN}(\mathbf{Z}_T^S, \mathbf{Z}_{T-1}^{s_0}; \mathbf{h}_T). \quad (10)$$

$\mathbf{Z}_T^{s_0}$ are also passed into the FFNs to obtain $\hat{\mathbf{b}}_{k_i,T}$ and $\hat{\mathbf{c}}_{k_i,T}$, respectively. Thus, the final output $\hat{\mathbf{Y}}_T$ of the FFNs consists of the predicted person bounding box and class pairs, Eq. (3). We use the set prediction loss (Carion et al. 2020) on $\hat{\mathbf{Y}}_T$. To compute the loss, a bipartite matching between the predictions and ground truth is required. We adopt a matching strategy similar to (Meinhardt et al. 2022), where we divide the ground truth $\mathbf{Y}_T = \{\mathbf{y}_{k_i,T}\}_{i=1}^M$ into two subsets based on their identities: 1) $\mathbf{Y}_{1,T} = \{\mathbf{y}_{k_i,T} \mid k_i \in \mathcal{K}_T \cap \mathcal{K}_{T-1}\}$, which represents people present in RGB pair frames $(\mathbf{x}_{T-1}, \mathbf{x}_T)$; and 2) $\mathbf{Y}_{2,T} = \{\mathbf{y}_{k_i,T} \mid k_i \in \mathcal{K}_T \setminus \mathcal{K}_{T-1}\}$, which represents newly detected people in the current RGB frame \mathbf{x}_T . For subset 1, we match the ground truth $\mathbf{y}_{k_i,T}$ to the prediction $\hat{\mathbf{y}}_{k_i,T}$ with the same identity, as person track embeddings from $T - 1$ carry over their identity to the subsequent frame T . In subset 2, we match the ground truth and prediction based on an injective minimum cost mapping in order to find the permutation τ with lowest cost (Carion et al. 2020):

$$\hat{\tau} = \arg \min_{\tau} \sum_{\mathbf{y}_i \in \mathbf{Y}_{2,T}} \mathcal{C}_{\text{match}}(\mathbf{y}_i, \hat{\mathbf{y}}_{\tau(i)}), \quad (11)$$

where $\mathcal{C}_{\text{match}}(\mathbf{y}_i, \hat{\mathbf{y}}_{\tau(i)})$ is the pairwise matching cost between the ground truth \mathbf{y}_i and prediction $\hat{\mathbf{y}}_{\tau(i)}$ with index $\tau(i)$. The ground truth subset \mathbf{Y}_2 is padded with \emptyset ($c_i = 0$, background class) such that it has the same size as the unmatched pairs, namely $(N_{\text{ns}} + N_{\text{tk}}) - |\mathcal{K}_T \cap \mathcal{K}_{T-1}|$. This matching cost is defined as:

$$\mathcal{C}_{\text{match}}(\mathbf{y}_i, \hat{\mathbf{y}}_{\tau(i)}) = \lambda_{\text{cls}} \hat{p}_{\tau(i)}(\hat{\mathbf{c}}_i) + \lambda_{l_1} |\mathbf{b}_i - \hat{\mathbf{b}}_{\tau(i)}| + \lambda_{\text{glou}} \mathcal{C}_{\text{glou}}(\mathbf{b}_i, \hat{\mathbf{b}}_{\tau(i)}), \quad (12)$$

where λ_{cls} , λ_{l_1} , and λ_{glou} are weighting parameters, and $\mathcal{C}_{\text{glou}}$ is the generalized IoU loss (Rezatofighi et al. 2019). The optimal assignment of the ground truth subset \mathbf{Y}_2 is obtained with the Hungarian algorithm, which uses a cost matrix based on the matching cost (Kuhn 1955).

After obtaining the optimal assignments, the final loss, \mathcal{L}_{MOT} , is computed. \mathcal{L}_{MOT} is the set prediction loss computed over all the output person bounding box predictions $\hat{\mathbf{Y}}_T = \{\hat{\mathbf{y}}_{k_i,T}\}_{i=1}^{N_{\text{ns}}+N_{\text{tk}}}$:

$$\mathcal{L}_{\text{MOT}}(\mathbf{y}_i, \hat{\mathbf{y}}_{\tau(i)}) = \sum_{\mathbf{y}_i \in \mathbf{Y}_t} \lambda_{\text{cls}} \hat{p}_{\tau(i)}(\hat{\mathbf{c}}_i) \quad (13)$$

$$+ (\lambda_{l_1} |\mathbf{b}_i - \hat{\mathbf{b}}_{\tau(i)}| + \lambda_{\text{glou}} \mathcal{C}_{\text{glou}}(\mathbf{b}_i, \hat{\mathbf{b}}_{\tau(i)})) \mathbf{1}_{c_i=1}.$$

The objective of the *Training Subsystem* is to minimize \mathcal{L}_{MOT} such that the predicted person bounding boxes and classes \mathbf{Y}_T from *LDTrack* closely align with the ground truth $\hat{\mathbf{Y}}_T$.

4 Datasets

We utilized multiple datasets to train and evaluate our people detection and tracking *LDTrack* architecture to include a variety of intraclass variations and environmental conditions. The following datasets were used for training:

1. The InOutdoor (IOD) Dataset (Mees et al. 2016) consisting of a total of 8,300 RGB-D images, each with a resolution of 950x540 pixels at 30 Hz. The dataset contains four image sequences of people, including groups of up to six people, walking under varying lighting conditions. Images were obtained from a Microsoft Kinect sensor mounted on the top of a mobile robot in both an indoor and outdoor campus environment. The first three sequences were used for training, and the last sequence was used for testing.

2. Kinect Tracking Precision (KTP) Dataset (Munaro and Menegatti 2014) consists of 8,475 RGB images with a resolution of 640x480 pixels at 30 Hz. The images are obtained from a side-mounted Microsoft Kinect sensor on a mobile robot in an indoor office environment. The dataset contains four RGB sequences representing arc, still, rotation, and translation robot motion patterns. A total of 14,766 instances of people are in the dataset, with groups as large as five individuals. The individuals are often partially occluded by others and self-occluded.

3. ISRT Tracking (ISRT) Dataset (Pereira et al. 2022) consists of 10,000 RGB images with a resolution of 640x480 pixels at 30 Hz. The images are obtained from an Intel RealSense D435 sensor mounted on a mobile robot in an indoor university campus setting. The dataset includes annotations for ten different object classes, including a person class. For training, we only considered the labels corresponding to people. We used odd-numbered sequences for training, and even-numbered sequences for testing (Pereira et al. 2022). However, for testing, we specifically selected a subset of sequences that contain people (e.g., 4, 6, and 12). The dataset contains groups of up to five people with scenarios of people occluding each other, body part occlusions, objects occluding individuals, and diverse poses such as sitting, leaning and standing.

4. Robots in Crowded People Conferences (R-CPC) Dataset: We collected our own R-CPC dataset from three different indoor university campus conferences using a mobile robot developed in our lab. A ZED Mini camera was mounted on each side of the robot (four in total), Fig. 2. The R-CPC dataset consists of 2,575 RGB-D images from each camera, all with a resolution of 640x480 pixels at 30 Hz. The Train Set 1 and Test Set 1 include

scenarios of the robot guiding a crowd of people from a main lobby down a corridor in a building. Set 1 consists of a total of 408 (for training) and 277 (for testing) images with 3,368 and 1,452 instances of people, respectively. The Train Set 2 and Test Set 2 include the robot moving within crowds of people that are walking, standing, and sitting at a conference. Set 2 consists of a total of 370 (for training) and 331 images (for testing) with 2,738 and 2,294 instances of people. Lastly, the Train Set 3 and Test Set 3 include scenarios of a robot guiding crowds of people from the main entrance of a building to a large poster room, where the robot also moves among the presenting attendees. Set 3 consists of a total of 808 (for training) and 380 (for testing) images with 4,713 and 2,603 instances of people.

The R-CPC dataset uniquely contains dense crowds of up to 18 people per frame. It also includes: 1) self-occlusions, partial occlusions, and full occlusions in both large open areas and within narrow corridors; 2) frequent short-term full occlusions as individuals momentarily walk in front of the camera; 3) frequent crossings where paths of multiple people intersect; 4) motion blurs due to rapid movements of individuals; 5) large and small objects occluding individuals (e.g., tables and chairs) and conference equipment (e.g., laptops, monitors); 6) pose variations (e.g., standing, bending over, sitting, and clothing deformations (e.g., jackets, backpacks, shoulder bags); and 7) a wide range of lighting conditions, from dim to bright environments due to the presence of both natural and artificial lighting sources.



Fig. 2 Mobile robot used to collect the R-CPC Dataset.

5 Training

LDTrack was trained using the *Training Subsystem* discussed in Section 3.2. We used a batch size of 1, and learning rates for the CNN and transformer network of 0.00001 and 0.0001, respectively (Carion et al. 2020). The weighting parameters λ_{cls} , λ_{l1} ,

and λ_{IoU} were set to 2, 5, and 2 (Carion et al. 2020). For the MLP in the *LFEN* module, we used a latent dimension $D = 288$. We select this dimension size to ensure compatibility with the transformer decoder. We select $N_{ns} = 500$ as it provides the optimal balance between detection accuracy and number of refinement steps for the reverse diffusion process (Chen et al. 2023). *LDTrack* was trained and validated separately on each of the four datasets with early stopping. Training took place on a workstation with two RTX 3070 GPUs, an AMD Ryzen Threadripper 3960X, and 128GB of memory.



Fig. 3 Example Images from the R-CPC Dataset.

6 Experiments

The objective of the experiments was to: 1) investigate the tracking accuracy and precision of *LDTrack* under intraclass variations, 2) compare our *LDTrack* with state-of-the-art (SOTA) robot people tracking methods, and 3) conduct an ablation study to validate the design choices of our architecture. The environments used in the experiments included varying levels of person occlusion, illumination, and deformation.

6.1 Performance Metrics

We used the CLEAR MOT (Bernardin and Stiefelhagen 2008) evaluation metrics, a standard evaluation tool which have been designed for assessing object tracking performance. The CLEAR MOT metrics we use herein are:

1. **Multiple Object Tracking Precision (MOTP)**: MOTP measures the average overlap between the ground truth and predicted people bounding boxes:

$$\frac{\sum_{i=1}^{N_{match}} \text{IoU}(\mathbf{b}_i, \hat{\mathbf{b}}_i)}{N_{match}}, \quad (14)$$

where N_{match} is the total number of matches between the ground

truth and prediction. A higher MOTP value, up to 100, indicates that the predicted person bounding boxes more closely match the actual person locations.

2. Multiple Object Tracking Accuracy (MOTA): MOTA measures tracking performance by taking into account the number of: false positives N_{fp} , false negatives N_{fn} , identity switches N_{IDSW} (when two tracked individuals mistakenly swap their identities), and ground truth person boxes N_{GT} :

$$MOTA = 1 - (N_{FP} + N_{FN} + N_{IDSW}) / N_{GT}. \quad (15)$$

A MOTA value close to 100 indicates high tracking accuracy.

6.2 Comparison Methods

We compared *LDTrack* with the following RGB SOTA people tracking methods for mobile robots:

1. SORT and Deep SORT (Pereira et al. 2022): SORT and Deep-SORT both use the YOLOv3 detector to identify bounding boxes of people in RGB images. KF is used for motion prediction and the Hungarian algorithm is used for data association. These methods are selected as they have achieved the highest object and people tracking accuracy and precision with varying levels of partial occlusions in the ISRT dataset (Pereira et al. 2022).

2. REGROUP (Taylor and Riek 2022): REGROUP also uses YOLOv3 to detect people in RGB images, a KF for motion prediction, and a CNN for appearance-based data association. REGROUP was selected as its Crowd Indication Feature can provide accurate discrimination of individual spatial positions within crowds of people (Pereira et al. 2022).

3. STARK (Pinto et al. 2023): STARK uses YOLOv3 for detection and KF for motion prediction. A person re-identification feature extractor is incorporated using TriNet (Yuan et al. 2020) which uses a ResNet backbone to output descriptors that capture variations in human appearance. Re-identification of people can improve person identification during occlusions (Pinto et al. 2023).

In addition to RGB methods, we compared our tracking performance results to people tracking methods which use additional depth information to investigate whether depth has a significant influence as an additional mode. Specifically, we compare with available reported results for the KTP dataset, *e.g.*,

Munaro *et al.* and Sun *et al.* (Munaro and Menegatti 2014; S. Sun et al. 2019).

4. Munaro *et al.* (Munaro and Menegatti 2014): This method uses RGB-D data with depth-based sub-clustering and HOG detection for tracking people using an Unscented KF (UKF) for position and velocity estimation and the Mahalanobis distance for data association. We choose this method as the use of a constant velocity model in the UKF allows for continuous tracking under temporary occlusions.

5. Sun *et al.* (S. Sun et al. 2019): RGB-D data is used within a Deformable Parts Model (DPM) for person detection and a Gaussian model is used to identify partially occluded people. A KF is used motion prediction and the Mahalanobis distance is used for data association. The method is able to effectively track individuals in scenarios with partial occlusions by evaluating depth values against a predefined Gaussian distribution to distinguish between occluded and visible parts of the target.

6.3 People Tracking Comparison Results

The people tracking results for our proposed *LDTrack* method and all comparison methods are presented in Table 1. In general, *LDTrack* outperformed the other RGB and RGB-D SOTA for people tracking by mobile robots with respect to both MOTA and MOTP across all test sets. This included under partial occlusions (KTP, ISRT, R-CPC datasets), pose deformations (ISRT, R-CPC datasets), and varying lighting (IOD, R-CPC datasets).

In particular, *LDTrack* achieved a MOTA of: 1) 78.6 on the IOD dataset, which is a 37% to 146% improvement over the other methods; 2) 92.7 on the KTP dataset, a 5% to 62% improvement; 3) 80.9 on the ISRT dataset, a 17% to 113% improvement; and 4) 49.0, 43.9, and 57.7 on Test Set 1, 2, and 3 from the R-CPC dataset with a 28% to 89% improvement over the SOTA methods. These results are statistically significant. This shows that *LDTrack* can accurately identify and track individuals, distinguishing between different individuals as well as adapting to dynamic changes in person appearances in crowded and cluttered environments.

In general, the performance benefits of our *LDTrack* are due

Table 1 Tracking Accuracy Comparison of our Proposed Tracking Method versus Existing Tracking Methods

| Method | Dataset | IOD | | KTP | | ISRT | | R-CPC | | | | | |
|---|---------|-------------------|------|--------------------|------|-------------------------|------|----------------|------|----------------|------|----------------|------|
| | | Test Set Lighting | | Test Set Occlusion | | Test Set Occlusion/Pose | | Test Set 1 All | | Test Set 2 All | | Test Set 3 All | |
| | | MOTP | MOTA | MOTP | MOTA | MOTP | MOTA | MOTP | MOTA | MOTP | MOTA | MOTP | MOTA |
| <i>LDTrack</i> | | 83.1 | 78.6 | 93.1 | 92.7 | 82.8 | 80.9 | 83.9 | 49.0 | 80.6 | 43.9 | 81.6 | 57.7 |
| SORT (Pereira et al. 2022) | | 70.0 | 57.3 | 65.6 | 71.6 | 81.4 | 69.0 | 74.4 | 30.6 | 72.9 | 24.0 | 73.2 | 36.4 |
| DeepSORT (Pereira et al. 2022) | | 70.1 | 54.3 | 64.6 | 62.8 | 81.3 | 67.6 | 72.3 | 35.6 | 71.7 | 29.4 | 71.4 | 38.5 |
| STARK (Pinto et al. 2023) | | 70.1 | 52.5 | 64.5 | 63.3 | 81.2 | 67.1 | 72.1 | 29.5 | 71.0 | 23.2 | 71.4 | 35.6 |
| REGROUP (Taylor and Riek 2022) | | 71.0 | 32.0 | 64.6 | 57.3 | 81.2 | 38.0 | 75.3 | 38.4 | 67.1 | 32.9 | 74.9 | 41.2 |
| Munaro et al. (Munaro and Menegatti 2014) | | - | - | 84.2 | 86.1 | - | - | - | - | - | - | - | - |
| Sun et al. (S. Sun et al. 2019) | | - | - | 84.4 | 88.2 | - | - | - | - | - | - | - | - |

Note: all missing values above (denoted '-') were not reported.

to its track-conditioned latent diffusion model, which dynamically updates person track embeddings by incorporating temporal information. This allows the model to adapt to changes in person appearances in the RGB images due to partial occlusions, and varying poses and lighting conditions. In contrast, the SOTA methods, which all use TBD approaches, rely on static person feature embeddings obtained from the detector at each frame. Such static embeddings can fail to account for temporal continuity, and are unable to adapt to changes in person appearances over time. For example, in scenarios where an individual transitions from sitting to standing, or becomes increasingly occluded.

In crowded environments in the R-CPC dataset, our *LDTrack* method outperformed the other methods with respect to both MOTA and MOTP. This demonstrates the advantage of our method in generating person box embeddings that can be iteratively refined to adapt to configurations in environments of any density or complexity, thereby improving generalizability. The REGROUP method showed improved performance over the other comparison methods with respect to MOTA and MOTP across all test sets on the R-CPC Dataset, due to its use of the CIF as previously mentioned. However, our *LDTrack* method still outperformed this method across all metrics, demonstrating the effectiveness of our diffusion model approach.

Non-parametric Kruskal-Wallis tests were performed on all datasets, showing a statistically significant difference in MOTA and MOTP between all methods: MOTA: $H = 31.5$, $p < 0.001$; and MOTP: ($H = 42.5$, $p < 0.001$). Posthoc Dunn tests with Bonferroni correction applied showed *LDTrack* had both a statistically significant higher 1) MOTA, $p < 0.001$, with respect to SORT ($Z = 3.03$), DeepSORT ($Z = 3.92$), STARK ($Z = 4.08$), and REGROUP ($Z = 5.27$); and 2) MOTP, $p < 0.001$, with respect to SORT ($Z = 4.64$), DeepSORT ($Z = 4.79$), STARK ($Z = 5.53$), and REGROUP ($Z = 5.37$), respectively.

The *Munaro et al.* and *Sun et al.* RGB-D methods, outperformed the SOTA *RGB-only* methods with respect to both MOTA and MOTP on the KTP dataset. This is due to the depth information providing additional spatial information to help distinguish between overlapping people and objects in occluded settings. However, despite being an RGB-only method, our *LDTrack* method still outperformed these two RGB-D methods across all metrics due to the inclusion of person track embeddings in our architecture. As these embeddings are specific to each individual, they allow for effective differentiation and re-identification of people using only RGB data.

Fig. 4 presents example tracking results of our *LDTrack* method (row 1) compared to the SORT (row 2), DeepSORT (row 3), STARK (row 4) and REGROUP (row 5) methods under: 1) poor illumination on the IOD dataset, Fig. 4(a), 2) partial occlusions by people on the KTP dataset, Fig. 4(b), 3) different poses and partial occlusions by both people and objects on the

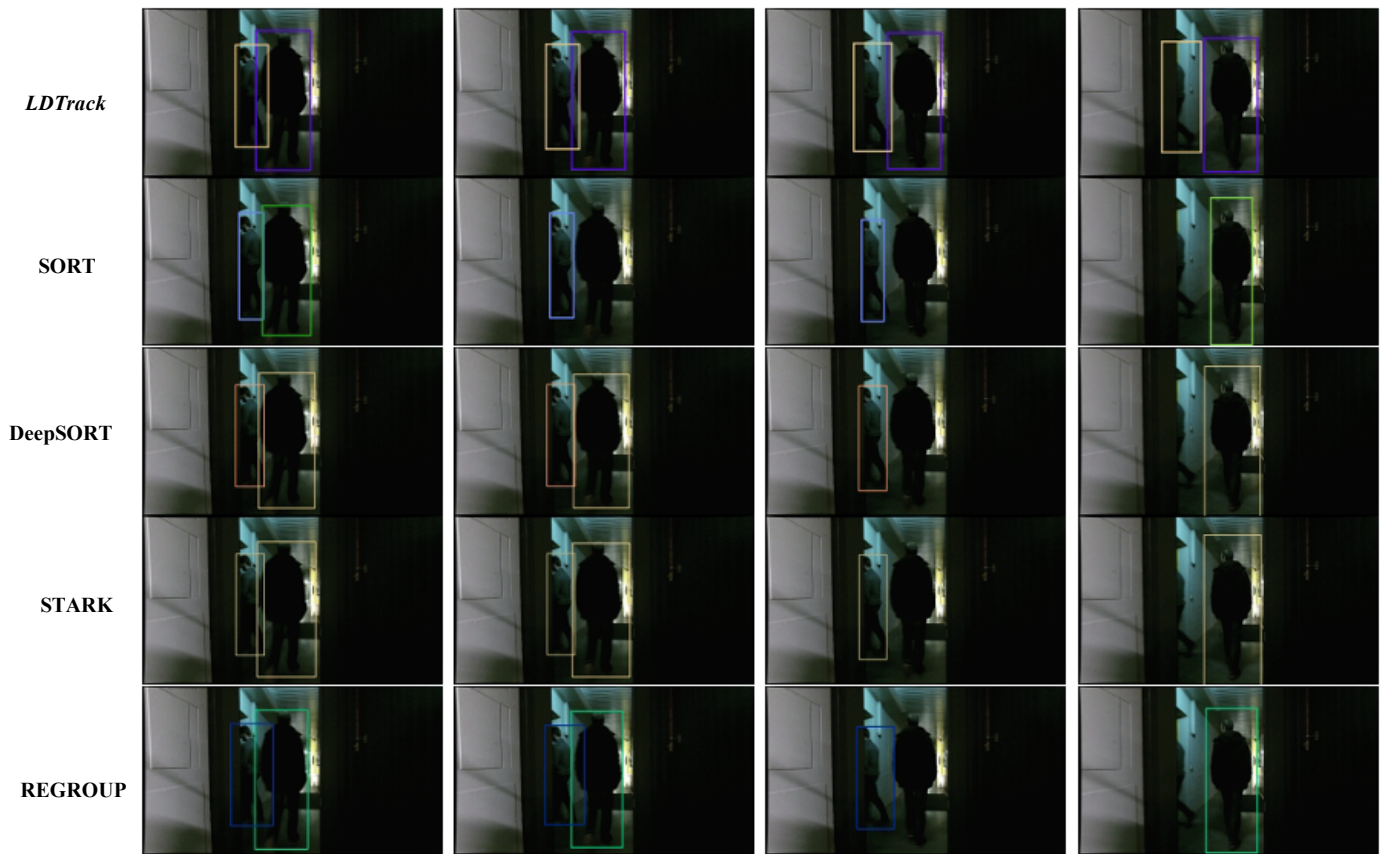
ISRT dataset, Fig. 4(c), and 4) varying poses and partial occlusions due to crowds on the R-CPC dataset, Fig. 4(d).

Fig. 4(a) represents a low-lighting scenario with two people walking in a hallway. The SOTA methods were unable to maintain consistent tracking, resulting in frequent loss of one or both people. In contrast, our *LDTrack* method was able to track the two people across all the consecutive frames. A scenario under partial occlusions is shown in Fig. 4(b) with two people on the left side of the images, one of whom is partially occluded by the other. There is an incorrect swap of the identity from the individual on the right to the one on the left in all the SOTA methods. Namely, the SORT and REGROUP methods, which do not consider appearance features such as clothing color and texture during data association, often resulted in identity swaps. While the DeepSORT and STARK methods do consider appearance features, they were unable to distinguish between the two individuals on the left due to similarities in their clothing. However, our *LDTrack* method was able to track both people consistently as distinct individuals since it explicitly considers temporal embedding information. Fig. 4(c) includes a scene with people in sitting and leaning positions with occlusion by furniture/equipment or other people. The SORT, DeepSORT, and STARK methods only detected the upper portion of the foremost person, who was partially occluded by an experimental set-up. Unfortunately, the lower portion of the person was not detected in the bounding box. The REGROUP method incorrectly detected the upper and lower portions of this foremost person as separate people. However, our *LDTrack* was able to infer the continuity of the foremost partially occluded person as represented by one bound box. Fig. 4(d) presents a crowded environment where only the *LDTrack* method was able to successfully track all 9 individuals present, including the fourth person in the forefront from the left (*i.e.*, defined by the lavender bounding box), who varies their pose from bending over the table (away from the camera, frames 1-3), to standing (frame 4). In contrast, the other methods misidentify this person in different poses as separate people (by assigning different identities) across the frames.

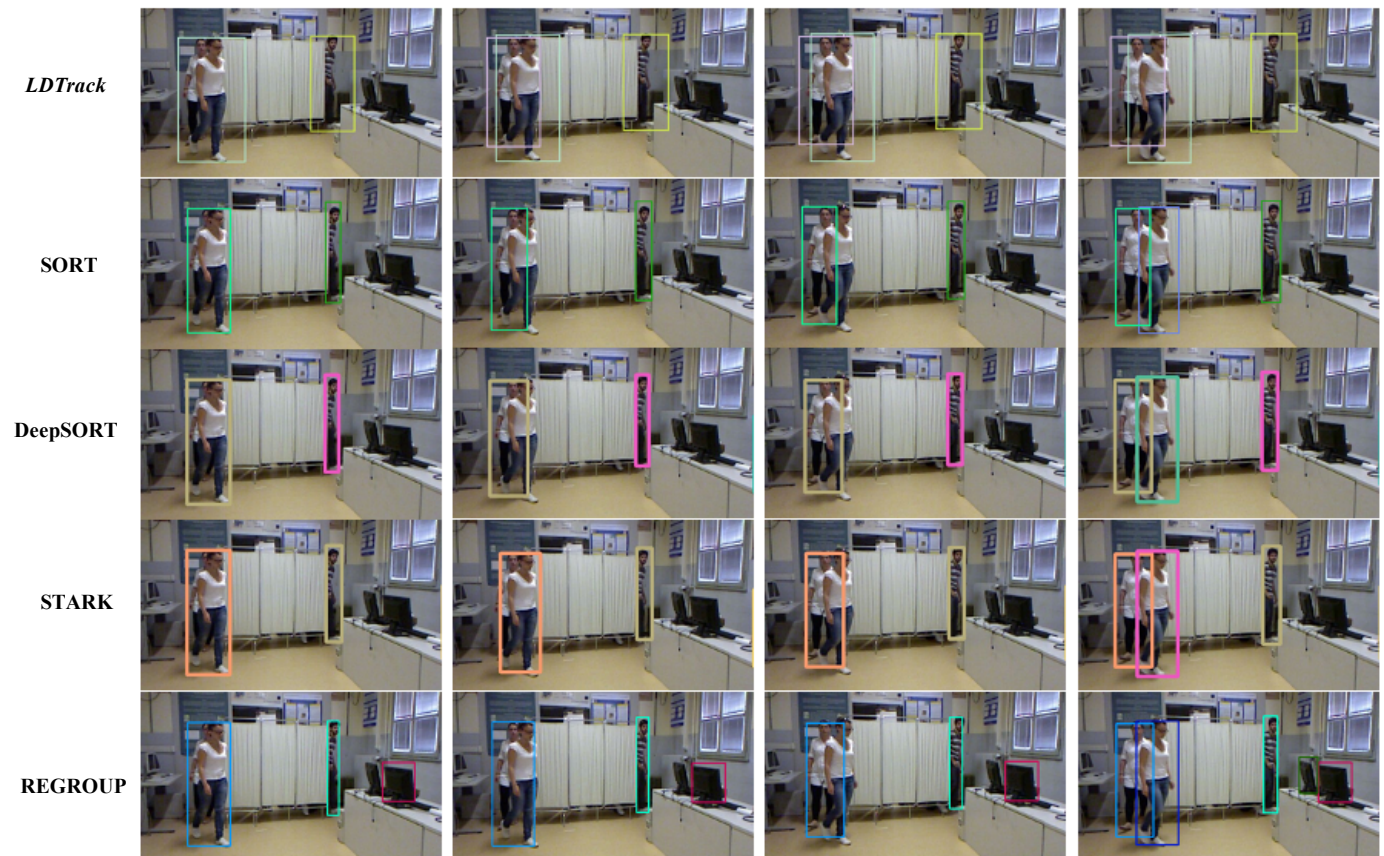
We conducted a further analysis by comparing our *LDTrack* method with the SOTA methods using a modified version of MOTP, which we identify as MOTP*. We considered MOTP* as it explicitly considers missed detections, whereas MOTP only measures the precision of detected individuals, Eq. (14). This is particularly important in cluttered and crowded environments where missed detections due to occlusions can frequently occur. MOTP* is represented as:

$$\sum_{i=1}^{N_{\text{match}}} \text{IoU}(\mathbf{b}_i, \widehat{\mathbf{b}}_i) / N_{\text{GT}}, \quad (16)$$

where an IoU value of zero is assigned for each missed detection.



(a) IOD Sequence



(b) KTP Sequence

Fig. 4 People tracking results for *LDTrack*, SORT, DeepSORT, STARK and REGROUP: (a) under poor illumination, (b) partial occlusion



Fig. 4 (continued) People tracking results for *LDTrack*, *SORT*, *DeepSORT*, *STARK* and *REGROUP*: (c) with different poses and partial occlusions, and (d) varying poses and partial occlusions due to crowds.

Applying MOTP* to all methods on the aforementioned IOD, KTP, ISRT, and R-CPC datasets in scenarios with person occlusions in dense crowds, significant improvements of *LDTrack* over the SOTA methods was observed, Table 2. In particular, on the R-CPC dataset, *LDTrack* obtained a MOTP* of 58.5 on Test Set 1, whereas SORT, DeepSORT, STARK, and REGROUP obtained a MOTP* of 30.1, 38.2, 40.9, and 40.0, respectively. Namely, there was a 44% to 94% improvement for *LDTrack* over the other methods. A non-parametric Kruskal-Wallis test was performed on all datasets, showing a statistically significant difference in MOTP* between all methods ($H = 28.9$, $p < 0.001$). Posthoc Dunn tests with Bonferroni correction applied showed our method had a statistically significant higher MOTP*, $p < 0.001$, with respect to SORT ($Z = 3.89$), DeepSORT ($Z = 3.68$), STARK ($Z = 4.32$) and REGROUP ($Z = 4.72$), respectively.

6.4 Ablation Study

We also performed an ablation study to evaluate the person track embedding design choice for the *LDTrack* architecture. Namely, we investigated whether varying the number of person track embeddings $\mathbf{Z}_T^{s_0}$ as inputs to the *ITRN* module during inference had a direct effect on accuracy and precision. We varied the number of person track embeddings from $N = 1$ to $N = 5$. For $N = 1$, which is our current approach, we used only $\mathbf{Z}_{T-1}^{s_0}$ as input, which is the person track embeddings from the last time step $T - 1$; for $N = 2$, we used both $\mathbf{Z}_{T-1}^{s_0}$ and $\mathbf{Z}_{T-2}^{s_0}$, following this procedure until $N = 5$, where we included all embeddings from $\mathbf{Z}_{T-1}^{s_0}$ to $\mathbf{Z}_{T-5}^{s_0}$ as inputs. Each person track, with identity k , is associated with multiple embeddings $\{\mathbf{Z}_{T-i}^{s_0}\}$, $i \in \{1, 2, \dots, N\}$ with each embedding $\mathbf{Z}_{T-i}^{s_0}$ generating a person bounding box prediction $\hat{\mathbf{b}}_{k,T-i}$ with classification score $p(\hat{\mathbf{c}}_{k,i-1})$. We selected the embedding with the highest classification score as the final person bounding box prediction, e.g., $\hat{\mathbf{b}}_{k,T_{\text{final}}} = \max_i \{\mathbf{Z}_{T-i}^{s_0}\}$. The results are presented in Table 3. Table 3 shows that increasing the number of person track embeddings had little impact on both MOTA and MOTP. This can be attributed to the fact that these embeddings are continuously adapted and repressed over time through our *ITRN* module. Therefore, the per-

son track embeddings from the most recent timestep $T - 1$ incorporates all the relevant information regarding a person’s appearance.

Table 2 Comparison of MOTP* of our Proposed Tracking Method versus Existing Tracking Methods

| Method \ Dataset | IOD | KTP | ISRT | R-CPC | | |
|------------------|-------------------|---------------|--------------------|----------------|----------------|----------------|
| | Test Set Lighting | Test Set Occ. | Test Set Occ./Pose | Test Set 1 All | Test Set 2 All | Test Set 3 All |
| | MOTP* | MOTP* | MOTP* | MOTP* | MOTP* | MOTP* |
| <i>LDTrack</i> | 77.5 | 91.7 | 69.2 | 58.5 | 52.6 | 54.8 |
| SORT | 59.6 | 58.0 | 65.5 | 30.1 | 23.2 | 34.2 |
| DeepSORT | 62.9 | 55.4 | 65.3 | 38.2 | 31.4 | 38.8 |
| STARK | 62.6 | 55.9 | 65.4 | 40.9 | 34.4 | 39.9 |
| REGROUP | 61.1 | 55.2 | 56.3 | 40.0 | 35.2 | 36.5 |

7 Conclusion

In this paper, we present a novel mobile robot person-tracking architecture, *LDTrack*, which directly addresses intraclass variations through the unique use of conditional latent diffusion models. The diffusion process is implemented in latent space, enabling the spatial-temporal refinement of temporal person embeddings. These embeddings represent different individuals detected by a robot in a shared environment, adapting dynamically to changes in their appearance over time. Such adaptation is essential in cluttered and crowded environments, where the appearance of individuals can vary significantly over time due to factors such as occlusions, pose deformations, and lighting variations. This adaptation is achieved by conditioning the diffusion model on person track embeddings from the previous time step. Extensive experiments verified that our *LDTrack* outperforms existing state-of-the-art tracking methods for mobile robots in tracking dynamic people across multiple real-world crowded and cluttered environments. Future work will explore the integration of our previously developed contrastive learning approach TimCLR (Fung et al. 2023), to pretrain our SFEN network in order to learn person representations that are invariant under intraclass variations. We will also test this combined methodology in real-time on a mobile robot in cluttered environments.

Table 3 Ablation Study

| Method \ Dataset | IOD | | KTP | | ISRT | | R-CPC | | | | | |
|----------------------------|-------------------|------|--------------------|------|-------------------------|------|----------------|------|----------------|------|----------------|------|
| | Test Set Lighting | | Test Set Occlusion | | Test Set Occlusion/Pose | | Test Set 1 All | | Test Set 2 All | | Test Set 3 All | |
| | MOTP | MOTA | MOTP | MOTA | MOTP | MOTA | MOTP | MOTA | MOTP | MOTA | MOTP | MOTA |
| <i>LDTrack</i> ($N = 1$) | 83.1 | 79.7 | 93.1 | 92.7 | 82.8 | 80.9 | 83.9 | 49.0 | 80.6 | 43.9 | 81.6 | 57.7 |
| <i>LDTrack</i> ($N = 2$) | 83.1 | 79.7 | 92.4 | 92.0 | 82.9 | 80.5 | 84.0 | 49.1 | 80.9 | 42.4 | 81.9 | 56.2 |
| <i>LDTrack</i> ($N = 3$) | 83.0 | 79.1 | 92.5 | 91.9 | 82.9 | 80.7 | 84.0 | 48.7 | 81.0 | 44.7 | 82.0 | 55.8 |
| <i>LDTrack</i> ($N = 4$) | 83.0 | 79.1 | 92.5 | 91.9 | 82.8 | 81.3 | 84.1 | 48.7 | 81.0 | 42.3 | 81.9 | 56.4 |
| <i>LDTrack</i> ($N = 5$) | 83.0 | 79.2 | 92.5 | 91.7 | 82.9 | 81.1 | 84.2 | 48.8 | 81.1 | 43.2 | 81.9 | 56.8 |

8 Declarations

8.1 Funding

This work was supported by the Natural Sciences and Engineering Research Council of Canada (NSERC), AGE-WELL Inc., and the Canada Research Chairs (CRC) program.

8.2 Conflicts of interest/Competing interests

We have no known conflicts of interest.

8.3 Availability of Data and Material

The IOD, KTP, and ISRT datasets are available at:

- 1) [IOD](#) (Mees et al. 2016)
- 2) [KTP](#) (Munaro and Menegatti 2014)
- 3) [ISRT](#) (Pereira et al. 2022)

References

- Agrawal, K., & Lal, R. (2021). Person Following Mobile Robot Using Multiplexed Detection and Tracking. In V. R. Kalamkar & K. Monkova (Eds.), *Advances in Mechanical Engineering* (pp. 815–822). Singapore: Springer.
- Bernardin, K., & Stiefelhagen, R. (2008). Evaluating Multiple Object Tracking Performance: The CLEAR MOT Metrics. *EURASIP Journal on Image and Video Processing*, 2008(1), 1–10.
- Bewley, A., Ge, Z., Ott, L., Ramos, F., & Upcroft, B. (2016). Simple Online and Realtime Tracking. In *2016 IEEE International Conference on Image Processing (ICIP)* (pp. 3464–3468).
- Carion, N., Massa, F., Synnaeve, G., Usunier, N., Kirillov, A., & Zagoruyko, S. (2020). End-to-End Object Detection with Transformers. In A. Vedaldi, H. Bischof, T. Brox, & J.-M. Frahm (Eds.), *Computer Vision – ECCV 2020* (Vol. 12346, pp. 213–229). Cham: Springer International Publishing.
- Chaabane, M., Zhang, P., Beveridge, J. R., & O’Hara, S. (2021, June 6). DEFT: Detection Embeddings for Tracking. arXiv. <http://arxiv.org/abs/2102.02267>.
- Chen, S., Sun, P., Song, Y., & Luo, P. (2023). DiffusionDet: Diffusion Model for Object Detection. In *2023 IEEE/CVF International Conference on Computer Vision (ICCV)* (pp. 19773–19786). Presented at the 2023 IEEE/CVF International Conference on Computer Vision (ICCV), Paris, France: IEEE.
- Chuang, Z., Sifa, Z., Haoran, W., Ziqing, G., Wenchao, S., & Lei, Y. (2024, February 1). AttentionTrack: Multiple Object Tracking in Traffic Scenarios Using Features Attention. arXiv.
- Dai, Z., Cai, B., Lin, Y., & Chen, J. (2022). UP-DETR: Unsupervised Pre-training for Object Detection with Transformers. *IEEE Transactions on Pattern Analysis and Machine Intelligence*, 1–11.
- Dendorfer, P., Ošep, A., Milan, A., Schindler, K., Cremers, D., Reid, I., et al. (2021). MOTChallenge: A Benchmark for Single-Camera Multiple Target Tracking. *International Journal of Computer Vision*, 129(4), 845–881.
- Dworakowski, D., Fung, A., & Nejat, G. (2023). Robots Understanding Contextual Information in Human-Centered Environments Using Weakly Supervised Mask Data Distillation. *International Journal of Computer Vision*, 131(2), 407–430.

- Fung, A., Benhabib, B., & Nejat, G. (2023). Robots Autonomously Detecting People: A Multimodal Deep Contrastive Learning Method Robust to Intra-class Variations. *IEEE Robotics and Automation Letters*, 8(6), 3550–3557. Presented at the IEEE Robotics and Automation Letters.
- Gupta, S., Tolani, V., Davidson, J., Levine, S., Sukthankar, R., & Malik, J. (2020). Cognitive Mapping and Planning for Visual Navigation. *International Journal of Computer Vision*, 128(5), 1311–1330.
- He, K., Gkioxari, G., Dollár, P., & Girshick, R. (2017). Mask R-CNN. In *2017 IEEE International Conference on Computer Vision (ICCV)* (pp. 2980–2988). Presented at the 2017 IEEE International Conference on Computer Vision (ICCV).
- He, K., Zhang, X., Ren, S., & Sun, J. (2016). Deep Residual Learning for Image Recognition. In *2016 IEEE Conference on Computer Vision and Pattern Recognition (CVPR)* (pp. 770–778). Presented at the 2016 IEEE Conference on Computer Vision and Pattern Recognition (CVPR).
- Ho, J., Jain, A., & Abbeel, P. (2020). Denoising Diffusion Probabilistic Models. In *Advances in Neural Information Processing Systems* (Vol. 33, pp. 6840–6851). Curran Associates, Inc.
- Kollmitz, M., Eitel, A., Vasquez, A., & Burgard, W. (2019). Deep 3D perception of people and their mobility aids. *Robotics and Autonomous Systems*, 114, 29–40.
- Kuhn, H. W. (1955). The Hungarian method for the assignment problem. *Naval Research Logistics Quarterly*, 2(1–2), 83–97.
- Lin, T.-Y., Goyal, P., Girshick, R., He, K., & Dollár, P. (2020). Focal Loss for Dense Object Detection. *IEEE Transactions on Pattern Analysis and Machine Intelligence*, 42(2), 318–327. Presented at the IEEE Transactions on Pattern Analysis and Machine Intelligence.
- Liu, T., Sun, J. J., Zhao, L., Zhao, J., Yuan, L., Wang, Y., et al. (2022). View-Invariant, Occlusion-Robust Probabilistic Embedding for Human Pose. *International Journal of Computer Vision*, 130(1), 111–135.
- Liu, W., Anguelov, D., Erhan, D., Szegedy, C., Reed, S., Fu, C.-Y., & Berg, A. C. (2016). SSD: Single Shot Multi-Box Detector. In B. Leibe, J. Matas, N. Sebe, & M. Welling (Eds.), *Computer Vision – ECCV 2016* (pp. 21–37). Cham: Springer International Publishing.
- Lu, Z., Rathod, V., Votel, R., & Huang, J. (2020). RetinaTrack: Online Single Stage Joint Detection and Tracking. In *2020 IEEE/CVF Conference on Computer Vision and Pattern Recognition (CVPR)* (pp. 14656–14666). Presented at the 2020 IEEE/CVF Conference on Computer Vision and Pattern Recognition (CVPR), Seattle, WA, USA: IEEE.
- Lugmayr, A., Danelljan, M., Romero, A., Yu, F., Timofte, R., & Van Gool, L. (2022). RePaint: Inpainting using Denoising Diffusion Probabilistic Models. In *2022*

- IEEE/CVF Conference on Computer Vision and Pattern Recognition (CVPR)* (pp. 11451–11461). Presented at the 2022 IEEE/CVF Conference on Computer Vision and Pattern Recognition (CVPR), New Orleans, LA, USA: IEEE.
- Luo, R., Song, Z., Ma, L., Wei, J., Yang, W., & Yang, M. (2023, August 19). DiffusionTrack: Diffusion Model For Multi-Object Tracking. arXiv. <http://arxiv.org/abs/2308.09905>.
- Mees, O., Eitel, A., & Burgard, W. (2016). Choosing smartly: Adaptive multimodal fusion for object detection in changing environments. In *2016 IEEE/RSJ International Conference on Intelligent Robots and Systems (IROS)* (pp. 151–156). Presented at the 2016 IEEE/RSJ International Conference on Intelligent Robots and Systems (IROS), Daejeon, South Korea: IEEE.
- Meinhardt, T., Kirillov, A., Leal-Taixe, L., & Feichtenhofer, C. (2022). TrackFormer: Multi-Object Tracking with Transformers. In *2022 IEEE/CVF Conference on Computer Vision and Pattern Recognition (CVPR)* (pp. 8834–8844). Presented at the 2022 IEEE/CVF Conference on Computer Vision and Pattern Recognition (CVPR), New Orleans, LA, USA: IEEE.
- Munaro, M., & Menegatti, E. (2014). Fast RGB-D people tracking for service robots. *Autonomous Robots*, 37(3), 227–242.
- Murray, S. (2017). Real-Time Multiple Object Tracking - A Study on the Importance of Speed. *arXiv:1709.03572 [cs]*. <http://arxiv.org/abs/1709.03572>.
- Pang, L., Cao, Z., Yu, J., Guan, P., Chen, X., & Zhang, W. (2020). A Robust Visual Person-Following Approach for Mobile Robots in Disturbing Environments. *IEEE Systems Journal*, 14(2), 2965–2968.
- Pereira, R., Carvalho, G., Garrote, L., & Nunes, U. J. (2022). Sort and Deep-SORT Based Multi-Object Tracking for Mobile Robotics: Evaluation with New Data Association Metrics. *Applied Sciences*, 12(3), 1319.
- Pinto, V., Bettencourt, R., & Ventura, R. (2023). People Re-Identification in Service Robots. In *2023 IEEE International Conference on Autonomous Robot Systems and Competitions (ICARSC)* (pp. 44–49). Presented at the 2023 IEEE International Conference on Autonomous Robot Systems and Competitions (ICARSC), Tomar, Portugal: IEEE.
- Redmon, J., & Farhadi, A. (2018, April 8). YOLOv3: An Incremental Improvement. arXiv. <http://arxiv.org/abs/1804.02767>. Accessed 27 May 2022
- Rezatofighi, H., Tsoi, N., Gwak, J., Sadeghian, A., Reid, I., & Savarese, S. (2019). Generalized Intersection Over Union: A Metric and a Loss for Bounding Box Regression. In *2019 IEEE/CVF Conference on Computer Vision and Pattern Recognition (CVPR)* (pp. 658–

- 666). Presented at the 2019 IEEE/CVF Conference on Computer Vision and Pattern Recognition (CVPR).
- Rombach, R., Blattmann, A., Lorenz, D., Esser, P., & Ommer, B. (2022). High-Resolution Image Synthesis with Latent Diffusion Models. In *2022 IEEE/CVF Conference on Computer Vision and Pattern Recognition (CVPR)* (pp. 10674–10685). Presented at the 2022 IEEE/CVF Conference on Computer Vision and Pattern Recognition (CVPR), New Orleans, LA, USA: IEEE.
- Royer, E., Lhuillier, M., Dhome, M., & Lavest, J.-M. (2007). Monocular Vision for Mobile Robot Localization and Autonomous Navigation. *International Journal of Computer Vision*, 74(3), 237–260.
- Russakovsky, O., Deng, J., Su, H., Krause, J., Satheesh, S., Ma, S., et al. (2015). ImageNet Large Scale Visual Recognition Challenge. *International Journal of Computer Vision*, 115(3), 211–252.
- Sanz, D., Ahmad, A., & Lima, P. (2015). Onboard robust person detection and tracking for domestic service robots. In *Robot 2015: Second Iberian Robotics Conference* (pp. 547–559). Cham, Switzerland: Springer.
- Sohl-Dickstein, J., Weiss, E., Maheswaranathan, N., & Ganguli, S. (2015). Deep Unsupervised Learning using Nonequilibrium Thermodynamics. In *Proceedings of the 32nd International Conference on Machine Learning* (pp. 2256–2265). Presented at the International Conference on Machine Learning, PMLR.
- Sun, Pei, Kretzschmar, H., Dotiwalla, X., Chouard, A., Patnaik, V., Tsui, P., et al. (2020). Scalability in Perception for Autonomous Driving: Waymo Open Dataset. In *2020 IEEE/CVF Conference on Computer Vision and Pattern Recognition (CVPR)* (pp. 2443–2451). Presented at the 2020 IEEE/CVF Conference on Computer Vision and Pattern Recognition (CVPR).
- Sun, Peize, Cao, J., Jiang, Y., Zhang, R., Xie, E., Yuan, Z., et al. (2021, May 4). TransTrack: Multiple Object Tracking with Transformer. arXiv. <http://arxiv.org/abs/2012.15460>.
- Sun, S., Zhao, X., & Tan, M. (2019). Fast and Robust RGB-D Multiple Human Tracking Based on Part Model for Mobile Robots. In *2019 Chinese Control Conference (CCC)* (pp. 4525–4530). Presented at the 2019 Chinese Control Conference (CCC), Guangzhou, China: IEEE.
- Tan, A. H., Bejarano, F. P., Zhu, Y., Ren, R., & Nejat, G. (2023). Deep Reinforcement Learning for Decentralized Multi-Robot Exploration With Macro Actions. *IEEE Robotics and Automation Letters*, 8(1), 272–279. Presented at the IEEE Robotics and Automation Letters.
- Taylor, A., & Riek, L. D. (2022). REGROUP: A Robot-Centric Group Detection and Tracking System. In *2022 17th ACM/IEEE International Conference on Human-Robot Interaction (HRI)* (pp. 412–421). Presented at the 2022 17th ACM/IEEE International Conference on

- Human-Robot Interaction (HRI), Sapporo, Japan: IEEE.
- Vasquez, A., Kollmitz, M., Eitel, A., & Burgard, W. (2017). Deep Detection of People and their Mobility Aids for a Hospital Robot. In *2017 European Conference on Mobile Robots (ECMR)* (pp. 1–7). Presented at the 2017 European Conference on Mobile Robots (ECMR), Paris: IEEE.
- Viola, P., & Jones, M. (2001). Rapid object detection using a boosted cascade of simple features. In *Proceedings of the 2001 IEEE Computer Society Conference on Computer Vision and Pattern Recognition. CVPR 2001* (Vol. 1, p. I-511-I-518). Kauai, HI, USA: IEEE Comput. Soc.
- Vo, D. M., Jiang, L., & Zell, A. (2014). Real time person detection and tracking by mobile robots using RGB-D images. In *2014 IEEE International Conference on Robotics and Biomimetics (ROBIO 2014)* (pp. 689–694). Bali, Indonesia: IEEE.
- Voigtlaender, P., Krause, M., Osep, A., Luiten, J., Sekar, B. B. G., Geiger, A., & Leibe, B. (2019). MOTs: Multi-Object Tracking and Segmentation. In *2019 IEEE/CVF Conference on Computer Vision and Pattern Recognition (CVPR)* (pp. 7934–7943). Presented at the 2019 IEEE/CVF Conference on Computer Vision and Pattern Recognition (CVPR), Long Beach, CA, USA: IEEE.
- Wang, Haitong, Tan, A. H., & Nejat, G. (2024, February 9). NavFormer: A Transformer Architecture for Robot Target-Driven Navigation in Unknown and Dynamic Environments. arXiv. <http://arxiv.org/abs/2402.06838>.
- Wang, Hanxiao, Zhu, X., Gong, S., & Xiang, T. (2018). Person Re-identification in Identity Regression Space. *International Journal of Computer Vision*, *126*(12), 1288–1310.
- Weber, T., Triputen, S., Danner, M., Braun, S., Schreve, K., & Räscht, M. (2018). Follow Me: Real-Time in the Wild Person Tracking Application for Autonomous Robotics. In H. Akiyama, O. Obst, C. Sammut, & F. Tonidandel (Eds.), *RoboCup 2017: Robot World Cup XXI* (Vol. 11175, pp. 156–167). Cham: Springer International Publishing.
- Wojke, N., Bewley, A., & Paulus, D. (2017). Simple online and realtime tracking with a deep association metric. In *2017 IEEE International Conference on Image Processing (ICIP)* (pp. 3645–3649). Presented at the 2017 IEEE International Conference on Image Processing (ICIP).
- Xue, F., Chang, Y., Wang, T., Zhou, Y., & Ming, A. (2024). Indoor Obstacle Discovery on Reflective Ground via Monocular Camera. *International Journal of Computer Vision*, *132*(3), 987–1007.
- Yan, Y., Li, J., Qin, J., Zheng, P., Liao, S., & Yang, X. (2023). Efficient Person Search: An Anchor-Free Approach.

International Journal of Computer Vision, 131(7),
1642–1661.

Yuan, Y., Chen, W., Yang, Y., & Wang, Z. (2020). In Defense of the Triplet Loss Again: Learning Robust Person Re-Identification with Fast Approximated Triplet Loss and Label Distillation. In *2020 IEEE/CVF Conference on Computer Vision and Pattern Recognition Workshops (CVPRW)* (pp. 1454–1463). Presented at the 2020 IEEE/CVF Conference on Computer Vision and Pattern Recognition Workshops (CVPRW), Seattle, WA, USA: IEEE.

Zeng, F., Dong, B., Zhang, Y., Wang, T., Zhang, X., & Wei, Y. (2022). MOTR: End-to-End Multiple-Object Tracking with Transformer. In S. Avidan, G. Brostow, M. Cissé, G. M. Farinella, & T. Hassner (Eds.), *Computer Vision – ECCV 2022* (Vol. 13687, pp. 659–675). Cham: Springer Nature Switzerland.

Zhou, X., Koltun, V., & Krähenbühl, P. (2020). Tracking Objects as Points. In A. Vedaldi, H. Bischof, T. Brox, & J.-M. Frahm (Eds.), *Computer Vision – ECCV 2020* (pp. 474–490). Cham: Springer International Publishing.

Zhu, X., Su, W., Lu, L., Li, B., Wang, X., & Dai, J. (2021, March 17). Deformable DETR: Deformable Transformers for End-to-End Object Detection. arXiv. <http://arxiv.org/abs/2010.04159>.